Supporting Information for

Entropically-driven Melting of Cu-based 1D Coordination Polymers

Yuki Ohara[a], Taichi Nishiguchi[a], Xin Zheng[b], Shin-ichiro Noro[b], Daniel Packwood,[c] Satoshi Horike[c,d,e]

[a]Department of Synthetic Chemistry and Biological Chemistry, Graduate School of Engineering, Kyoto University, Katsura, Nishikyo-ku, Kyoto 615-8510, Japan
[b]Graduate School of Environmental Science, Hokkaido University, Sapporo 060-0810, Japan
[c]Institute for Integrated Cell-Material Sciences, Institute for Advanced Study, Kyoto University, Yoshida-Honmachi, Sakyo-ku, Kyoto 606-8501, Japan
[d]Department of Chemistry, Graduate School of Science, Kyoto University, Kitashirakawa-Oiwakecho, Sakyo-ku, Kyoto 606-8502, Japan
[e]Department of Materials Science and Engineering, School of Molecular Science and Engineering, Vidyasirimedhi Institute of Science and Technology, Rayong, 21210, Thailand

Synthesis of crystalline powders of $Cu(A)_2(L)_2$

All chemicals and solvents used in the synthesis were of reagent grade and used without further purification.

$Cu(TFSI)_2(bpp)_2$

Crystalline powders were synthesized according to the previous report.[1]

$Cu(Ms_2N)_2(bpp)_2$

Crystalline powders were synthesized according to the previous report.[1]

$Cu(TFSI)_2(bpe)_2$

Crystalline powders were synthesized as follows: 20 mmol HTFSI and 10 mmol $Cu(OH)_2$ were mixed in 100 ml H_2O and stirred at room temperature for 1 h. The mixture were evaporated, and dried at 80 °C for 6 h under vacuum, then blue powders were obtained. The obtained blue powders were dissolved in H_2O, then 50mL 0.1 M $Cu(TFSI)_2$ aqueous solution was prepared. The solution was mixed wth 50 mL 0.2 M bpp MeOH solution, and stirred at room temperature for 2 h. The purple precipitates were filtered and washed with MeOH, then dried at 80°C for 6 h under vacuum. Single

crystal of $Cu(TFSI)_2(bpe)_2$ was synthesized as follows: Purple single crystals were collected.

$Cu(BF_4)_2(bpp)_2$

Crystalline powders were synthesized according to the previous report.[2]

Single crystal X-ray diffraction and structure analysis

Single crystal X-ray diffraction measurements were performed using a Rigaku Micro Max-007 HF diffractometer and a Pilatus 200 K detector with Cu Kα radiation (λ = 1.54184 Å) at 173 K. The crystal structures were solved by using direct method (SHELXT)[3] and refined by using full-matrix least-squares techniques on F^2 using SHELXL-2018 (ver. 2018/3).[4]

Powder X-ray diffraction

Powder X-ray diffraction (PXRD) patterns were collected on a Rigaku SmartLab diffractometer with CuKα radiation (λ = 1.54 Å).

Elemental analysis

CHN elemental analysis was conducted on a MICRO CORDER JM11 (J-Science Lab Co., Ltd.).

Thermal property measurements

Thermogravimetry-differential thermal analysis (TG-DTA) was performed using a Rigaku Thermo plus TG 8120 apparatus in the temperature range between 25 and 500 °C with Ar gas flow (50-60 mL min^{-1}) and at the heating rate of 10 °C min^{-1}. Differential scanning calorimetry (DSC) was carried out with a Hitachi DSC7200 at the heating rate of 10 °C min^{-1}. Sample preparations for DSC were conducted under Ar. The ΔH_{fus} was calculated as an amount per sample weight by integrating the endothermic peak in the 1st heating of DSC profile, then converted to per molecular weight. Determination of T_m and peak integration were performed using the analysis software supplied with the equipment (Hitachi High-Tech NEXTA software).

Variable temperature Powder X-ray diffraction (VT-PXRD)

VT-PXRD patterns were collected on a Rigaku SmartLab diffractometer with CuKα radiation (λ = 1.54 Å) at temperatures between 30°C and 210°C for $Cu(TFSI)_2(bpp)_2$ and between 30°C and 180°C for $Cu(Ms_2N)_2(bpp)_2$. with N_2 gas flow (20 mL min^{-1}).

Variable temperature X-ray absorption spectroscopy (XAS)

Cu K-edge X-ray absorption spectroscopy (XAS) including X-ray absorption near

edge structure (XANES) and extended X-ray absorption fine structure (EXAFS) regions were performed in the transmission mode at BL14B2 beamline at SPring-8. Cu foil internal energy calibration was carried out before sample measurements. The sample was pelletized with boron nitride powder prior to the measurement. The temperature-dependent XAS study was performed by heating the sample under N_2. Variable temperature radial distribution function (VT-RDF) profiles were obtained from the analysis of EXAFS spectra by using Arthemis software.[5]

Density functional theory (DFT) calculations

DFT calculations were performed using the Vienna Ab initio Simulation Package (VASP),[6] using the projector augmented wave method (PAW) with a plane-wave basis set.[7] The rev-vdW-DF2 exchange-correlation functional[8] was used. The cutoff energy of 600 eV was used with a 3 × 2 × 1 Γ-centered k-point mesh. Gaussian smearing was employed with σ = 0.05 eV. The energy convergence threshold is set as 10^{-5} eV. 2 × 2 × 2 supercells were generated from the relaxed structures and used for calculation of chain-chain interaction ($E_{\text{chain-chain}}$). $E_{\text{chain-chain}}$ was computed as the energy difference per mole between isolated 1D chains (E_{chain}) and the crystal containing the same number of chains (E_{crystal}):

$$E_{\text{chain-chain}} = (E_{\text{crystal}} - \text{n}\, E_{\text{chain}})/(2\text{n})$$

where n is the number of chains in the crystal. In all cases, the supercells of crystal contains 8 chains (n = 8). As an example, the supercell of crystal and the isolated 1D chain of $Cu(TFSI)_2(bpp)_2$ are shown in Figure S5. E_{chain} and E_{crystal} were calculated by DFT in corresponding simulation cells with the same level of theory but without structural relaxation. Calculated E_{chain}, E_{crystal} and $E_{\text{chain-chain}}$ in each compound are shown in Table S2.

Discussion on the thermodynamic parameters in $Cu(TFSI)_2(bpp)_2$ and $Cu(BF_4)_2(bpp)_2$

Based on the discussion on the case of $Cu(TFSI)_2(bpp)_2$ and $Cu(Ms_2N)_2(bpp)_2$ or $Cu(TFSI)_2(bpe)_2$, the more complex cases of $Cu(TFSI)_2(bpp)_2$ (T_m = 196°C) and $Cu(BF_4)_2(bpp)_2$ (no melting) were investigated. For E_{ionic}, $Cu(BF_4)_2(bpp)_2$ is expected to have a larger E_{ionic} than $Cu(TFSI)_2(bpp)_2$ due to the smaller size of BF_4^-.[9] $E_{\text{chain-chain}}$, on the other hand, is 33 kJ mol^{-1} larger for $Cu(TFSI)_2(bpp)_2$ (Table 2). It is not possible to claim a larger or smaller relationship for ΔH_{fus} due to the opposite trend in E_{ionic} and $E_{\text{chain-chain}}$. For S_{kin}, based on the $E_{\text{chain-chain}}$ values, S_{kin} in the crystal was expected to be smaller for $Cu(TFSI)_2(bpp)_2$. In terms of S_{confor}, $TFSI^-$ can adopt multiple

conformations whereas BF_4^- adopts only a single conformation. S_{confor} in the liquid phase is expected to be larger for $Cu(TFSI)_2(bpp)_2$. For these reasons, ΔS_{fus} was expected to be higher in $Cu(TFSI)_2(bpp)_2$ than in $Cu(BF_4)_2(bpp)_2$. Considering that the effect of ΔH_{fus} derived from E_{ionic} and $E_{chain\text{-}chain}$ is small in this structural system, suggested in the study in other compounds, the effect of ΔS_{fus} increase is considered dominant in the T_m decrease in $Cu(TFSI)_2(bpp)_2$.

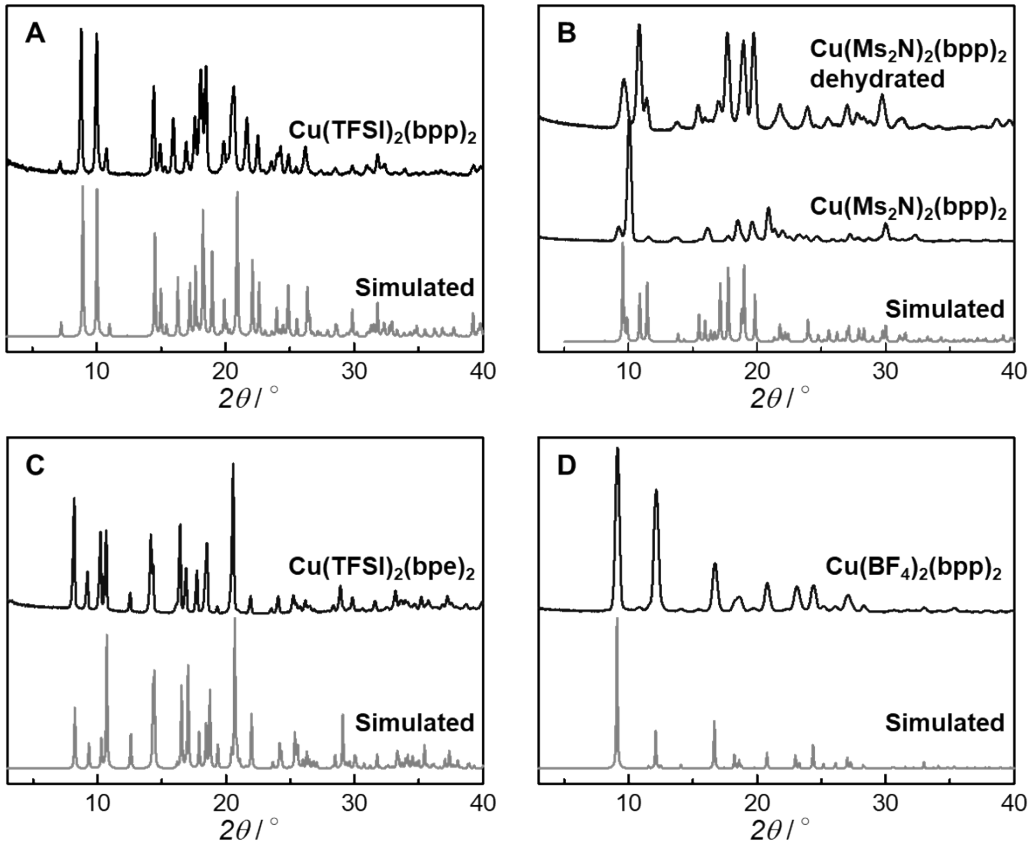

Figure S1. PXRD patterns of simulated and as-synthesized or degassed (A) $Cu(TFSI)_2(bpp)_2$, (B) $Cu(Ms_2N)_2(bpp)_2$, (C) $Cu(TFSI)_2(bpe)_2$ and (D) $Cu(BF_4)_2(bpp)_2$. For the dehydrated form of $Cu(Ms_2N)_2(bpp)_2$, the sample was degassed at 100°C and measured under inert atmosphere.

Table S1. Elemental analysis.

Compound	H (calcd) /%	H (found) /%	C (calcd) /%	C (found) /%	N (calcd) /%	N (found) /%
$Cu(TFSI)_2(bpp)_2$	2.77	2.70	35.31	35.11	8.24	8.43
$Cu(Ms_2N)_2(bpp)_2$	5.01	4.90	44.79	44.56	10.45	10.40
$Cu(TFSI)_2(bpe)_2$	4.45	4.40	49.28	49.45	8.84	8.66
$Cu(BF_4)_2(bpp)_2$	2.44	2.39	33.89	33.73	8.47	8.26

Table S2. Parameters of crystal structures of $Cu(TFSI)_2(bpe)_2$. CCDC deposited number is #2321776.

Compound	$Cu(TFSI)_2(bpe)_2$
Formula	$C_{28}H_{24}Cu_6F_{12}N_6O_8S_4$
MW (g/mol)	992.31
***T* (K)**	173
Wavelength (Å)	1.54187
Crystal system	Monoclinic
Space group	*C* 2
***a* (Å)**	19.966(6)
***b* (Å)**	9.159(2)
***c* (Å)**	11.301(4)
***β* (Å)**	108.602(9)
***V* (Å^3)**	1958.6(10)
Z	2
***ρ* (g cm^{-3})**	1.683
***μ* (mm^{-1})**	3.812
Number of collected/independent reflection	3438/3018
R_1, wR_2 [I□2σ(I)]	0.0278, 0.0592
R_1, wR_2 (all data)	0.0330, 0.0602
GOF	0.945

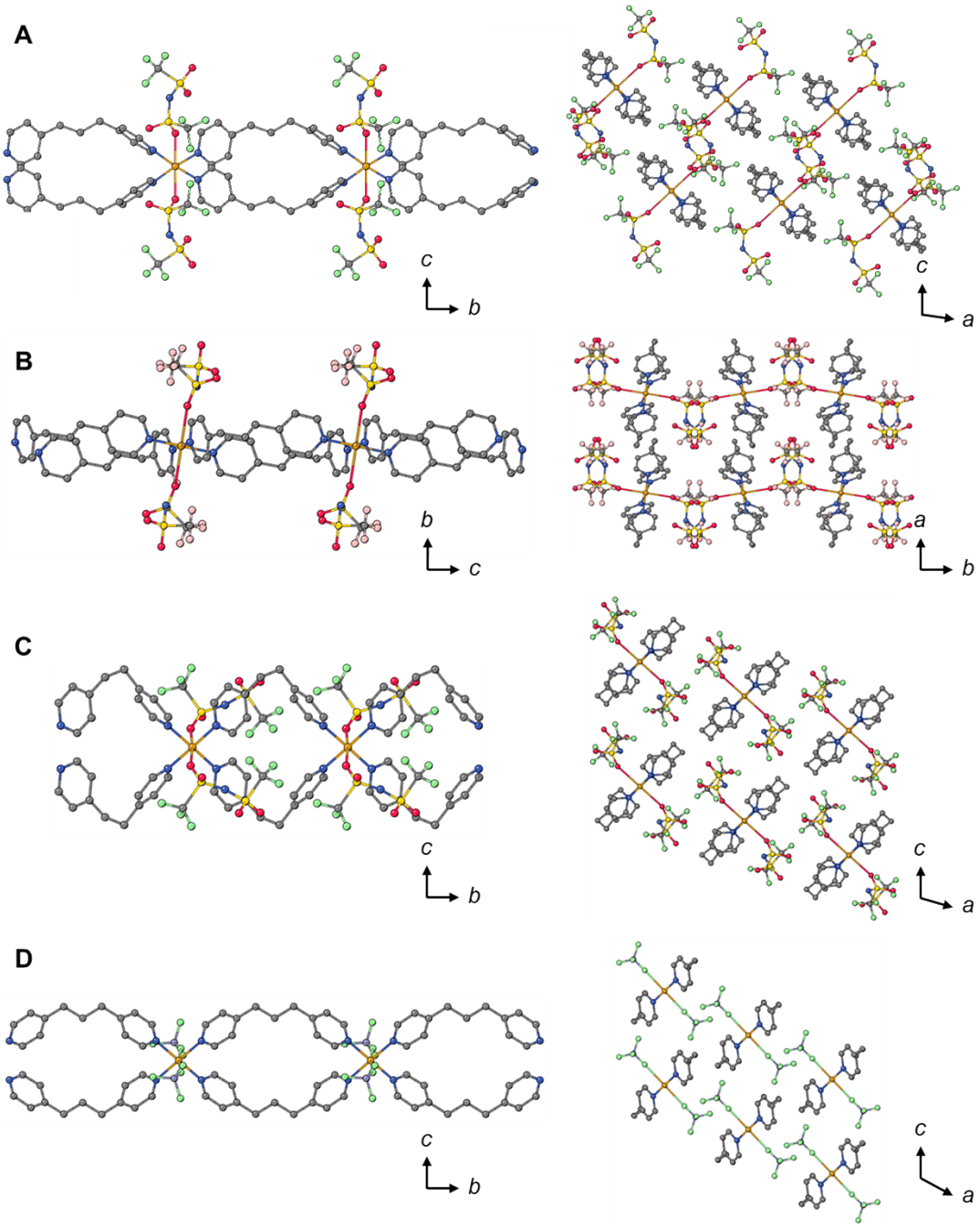

Figure S2. Crystal structure of the one-dimensional ribbon-chain and 3D packing structure of (A) $Cu(TFSI)_2(bpp)_2$, (B) $Cu(Ms_2N)_2(bpp)_2$ (C) $Cu(TFSI)_2(bpe)_2$. (D) $Cu(BF_4)_2(bpp)_2$. Orange, grey, blue, red, green, yellow, and purple spheres represent Cu, C, N, O, F, S and B atoms, respectively. H atoms have been omitted for clarity except for that of Ms_2N^- in $Cu(Ms_2N)_2(bpp)_2$.

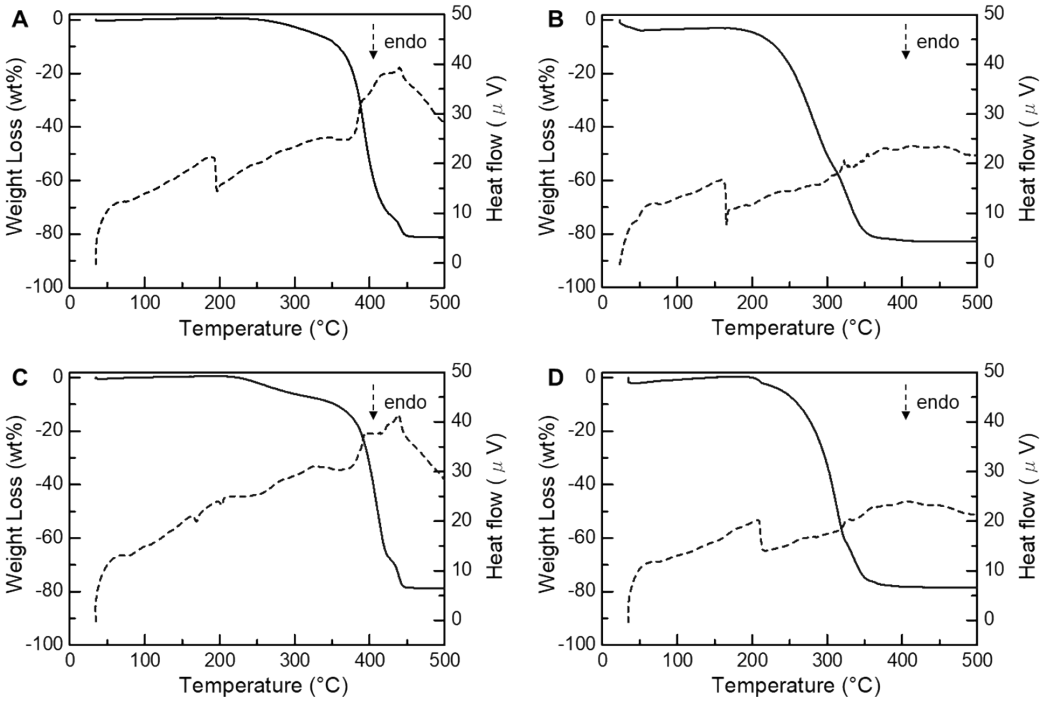

Figure S3. TG-DTA profiles of (A) $Cu(TFSI)_2(bpp)_2$, (B) $Cu(Ms_2N)_2(bpp)_2$, (C) $Cu(TFSI)_2(bpe)_2$, and (D) $Cu(BF_4)_2(bpp)_2$.

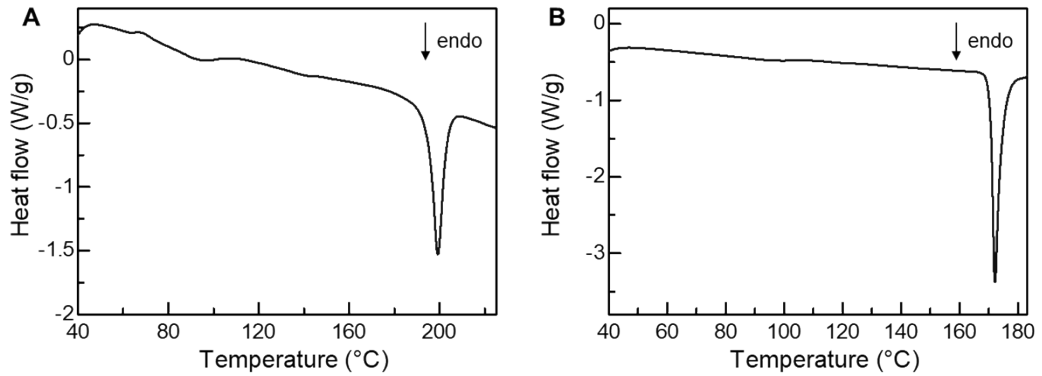

Figure S4. DSC profiles of (A) $Cu(TFSI)_2(bpp)_2$ and (B) $Cu(Ms_2N)_2(bpp)_2$.

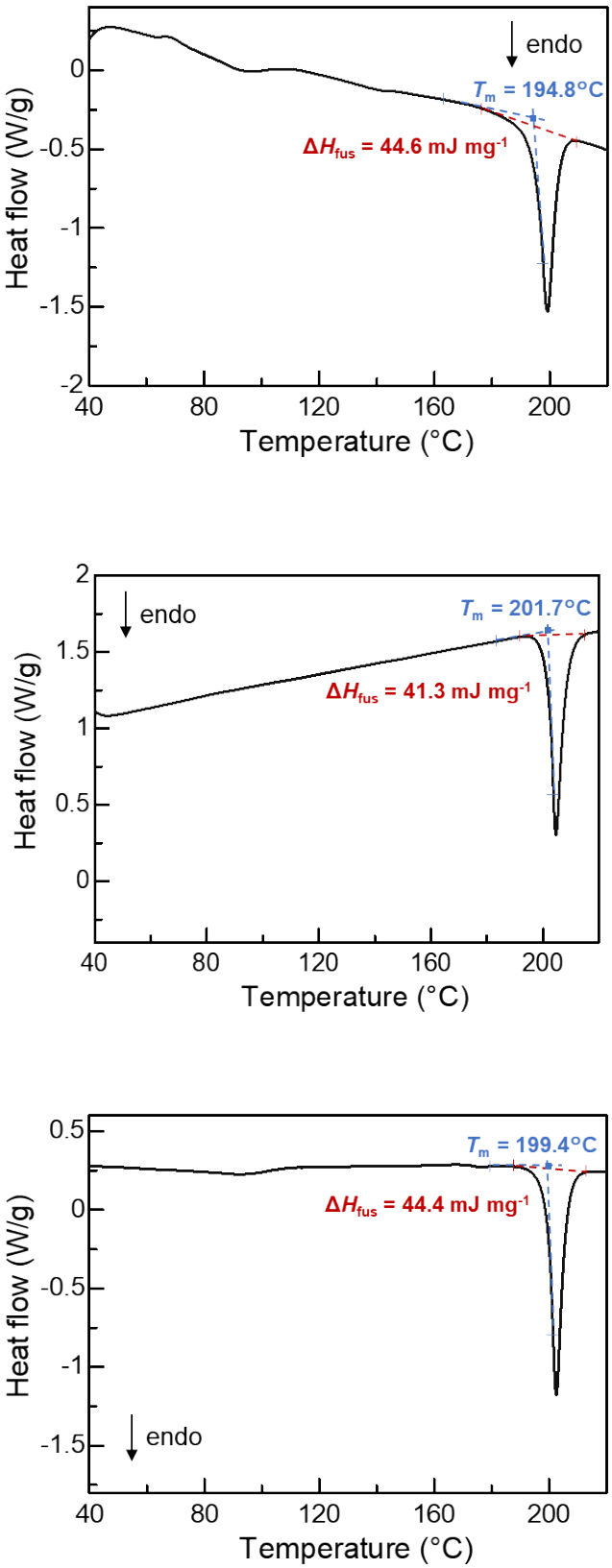

Figure S5. DSC profiles of $Cu(TFSI)_2(bpp)_2$ and determination of T_m and ΔH_{fus}. Measurements were conducted three times.

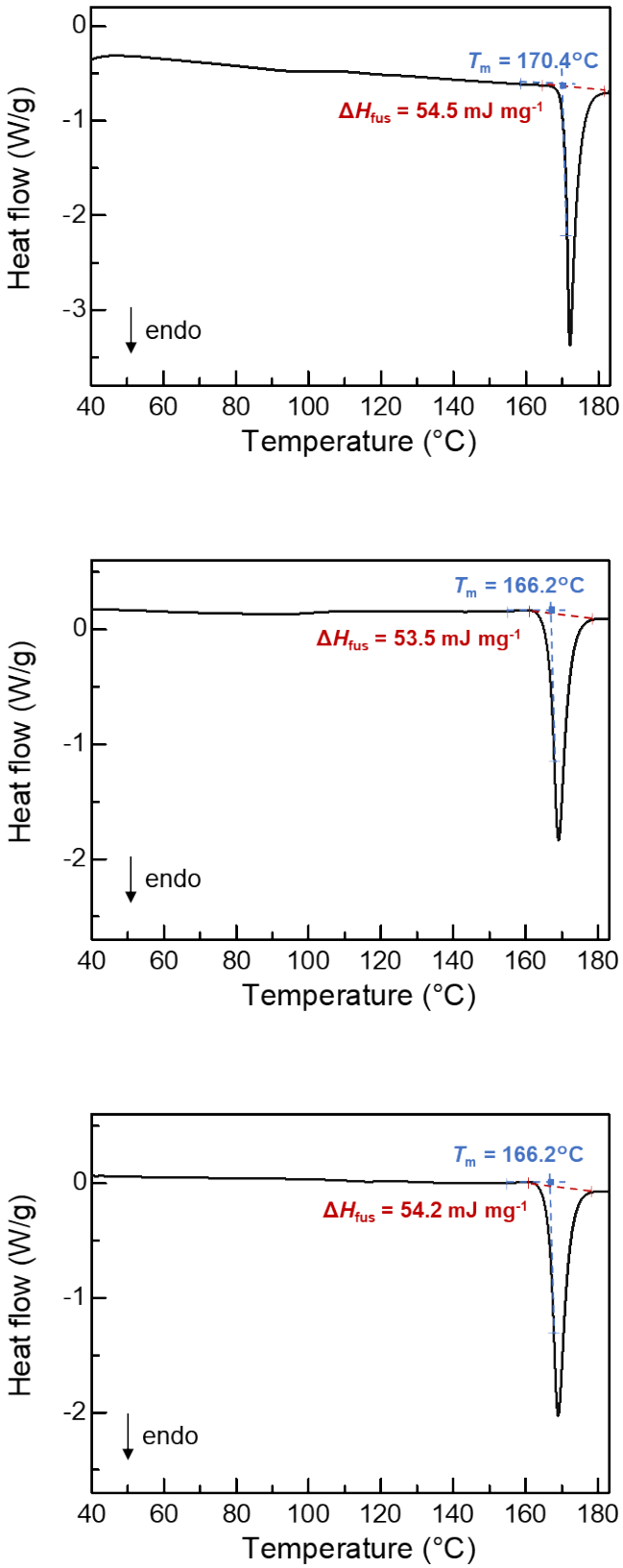

Figure S6. DSC profiles of $Cu(Ms_2N)_2(bpp)_2$ and determination of T_m and ΔH_{fus}. Measurements were conducted three times.

Table S3. T_m, ΔH_{fus}, and ΔS_{fus} for $Cu(TFSI)_2(bpp)_2$ and $Cu(Ms_2N)_2(bpp)_2$ determined by DSC measurements.

Compound		T_m / °C	ΔH_{fus} / mJ mg^{-1}	ΔH_{fus} / kJ mol^{-1}	ΔS_{fus} / J mol^{-1} K^{-1}
$Cu(TFSI)_2(bpp)_2$	Meas. 1	194.8	44.6	45.5	97.3
	Meas. 2	201.7	41.3	42.1	88.7
	Meas. 3	199.4	44.4	45.3	95.9
	Ave.	**198.6**	**43.4**	**44.3**	**94.0**
	S.D.	2.9	1.5	1.5	3.7
$Cu(Ms_2N)_2(bpp)_2$	Meas. 1	170.4	54.5	43.8	98.8
	Meas. 2	166.2	53.5	43.0	98.0
	Meas. 3	166.2	54.2	43.6	99.2
	Ave.	**167.6**	**54.1**	**43.5**	**98.7**
	S.D.	2.0	0.4	0.3	0.5

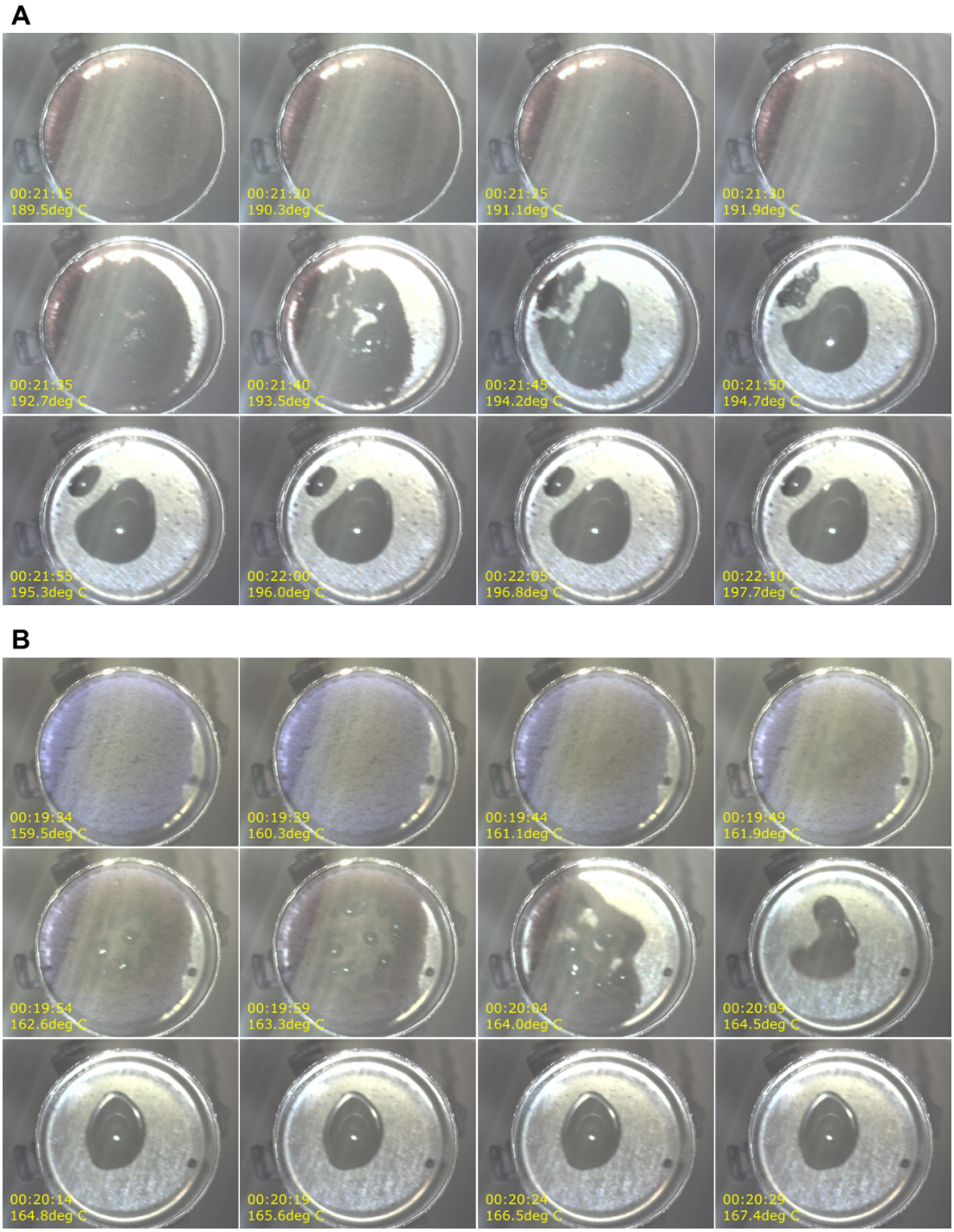

Figure S7. Microscope images of melting in TG-DTA measurement of (A) $Cu(TFSI)_2(bpp)_2$ and (B) $Cu(Ms_2N)_2(bpp)_2$.

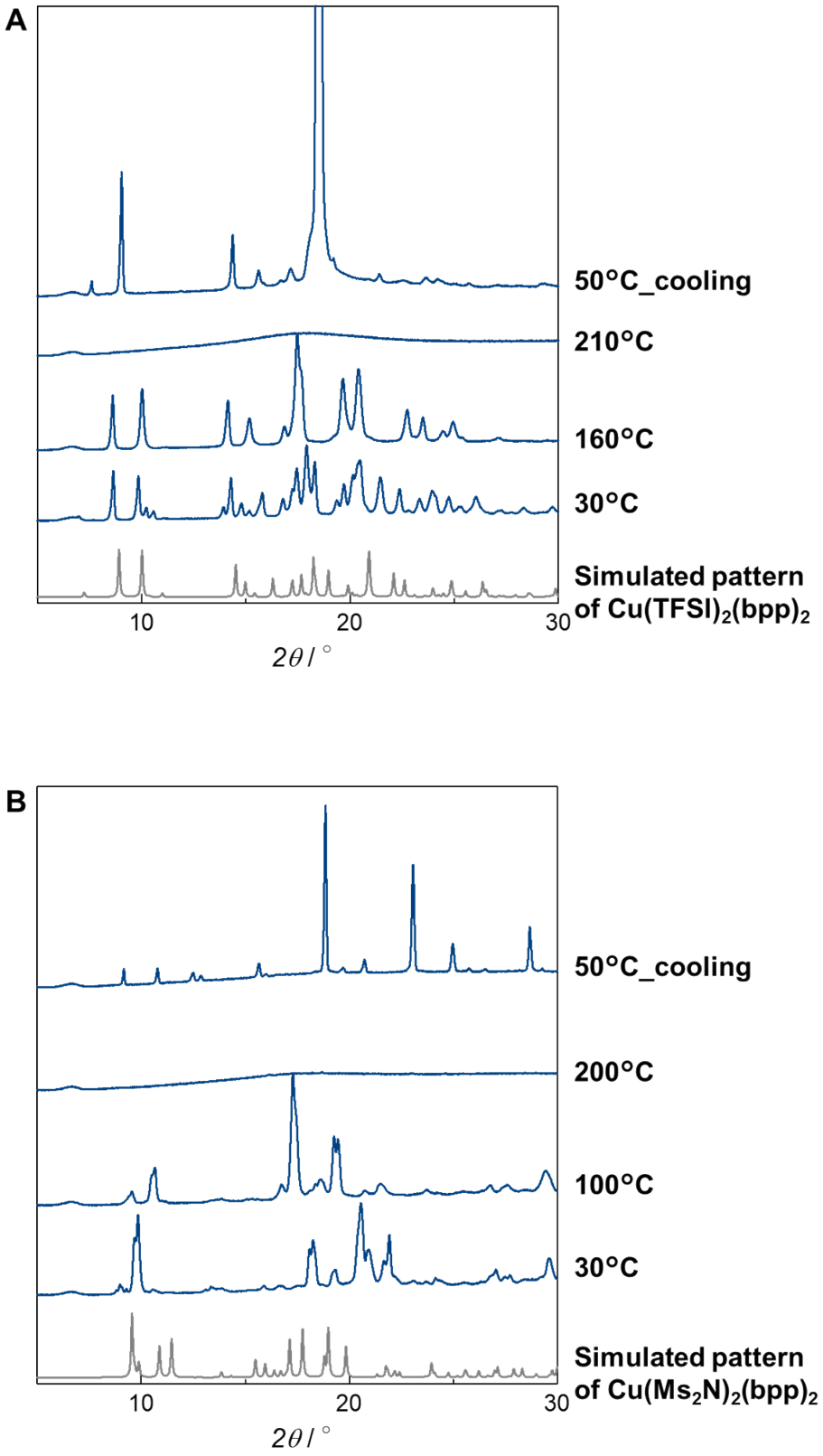

Figure S8. VT-PXRD patterns of (A) $Cu(TFSI)_2(bpp)_2$ and (B) $Cu(Ms_2N)_2(bpp)_2$.

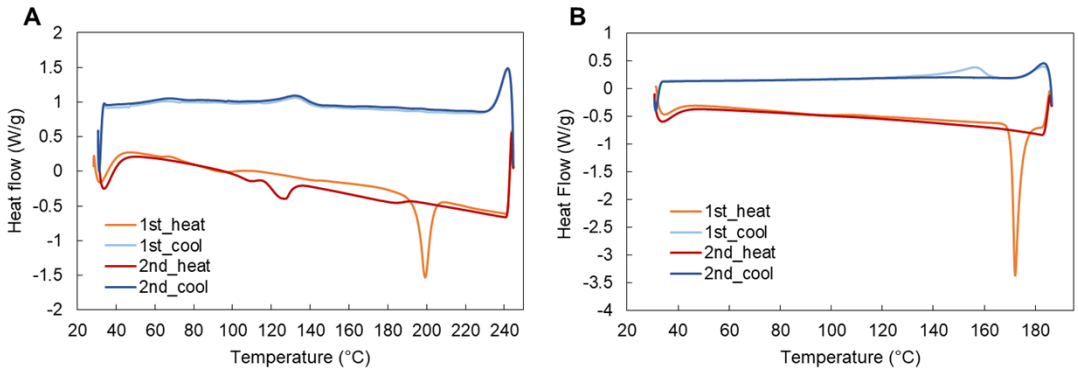

Figure S9. DSC profile with cooling and 2nd heating branches of (A) $Cu(TFSI)_2(bpp)_2$ and (B) $Cu(Ms_2N)_2(bpp)_2$.

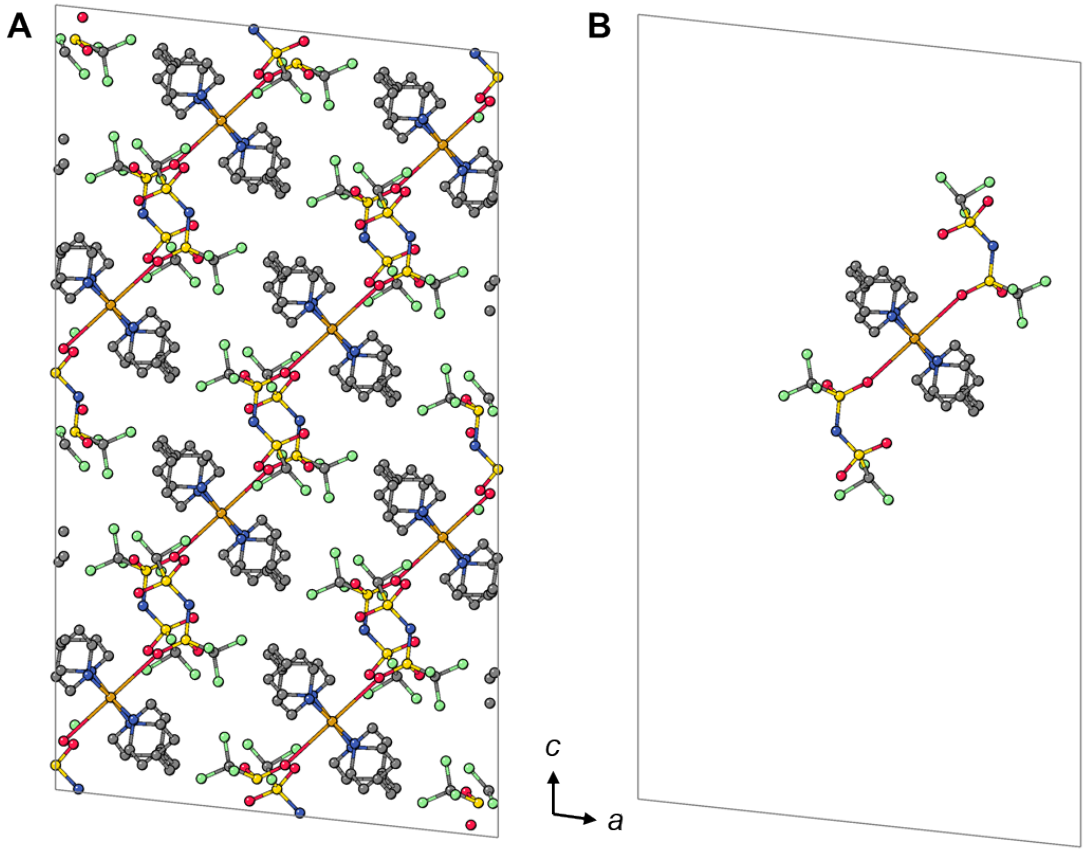

Figure S10. Simulation cell of (A) crystal and (B) isolated 1D chain in a 2 2 2 supercell in the $E_{chain\text{-}chain}$ calculations of $Cu(TFSI)_2(bpp)_2$.

Table S4. Calculated values E_{chain}, $E_{crystal}$ and $E_{chain\text{-}chain}$ in each compound.

	$Cu(TFSI)_2(bpp)_2$	$Cu(Ms_2N)_2(bpp)_2$	$Cu(TFSI)_2bpe)_2$	$Cu(TFSI)_2(BF_4)_2$
E_{chain} /eV	-1018.997	-1035.912	-954.883	-826.325
$E_{crystal}$ /eV	-8196.475	-8345.887	-7681.954	-6649.614
$E_{chain\text{-}chain}$ /kJ mol^{-1}	-268.3	-353.3	-258.7	-235.3

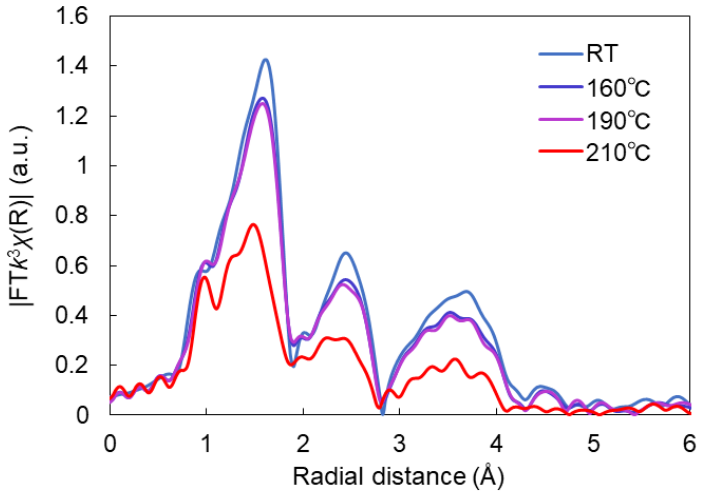

Figure S11. VT-RDF profiles of $Cu(TFSI)_2(bpp)_2$.

References

1. X. Zheng, K. Fukuhara, Y. Hijikata, J. Pirillo, H. Sato, K. Takahashi and S. Noro, *Commun*. *Chem*. 2020, **3**, 143.

2. T. Suzuki, R. Kotani, A. Kondo and K. Maeda, *J*. *Phys*. *Chem*. *C*, 2016, **120**, 21571–21579.

3. G. M. Sheldrick, SHELXT–Integrated space-group and crystal-structure determination. *Acta Cryst.* 2015, A**71**, 3–8.

4. G. M. Sheldrick, Crystal structure refinement with SHELXL. *Acta Cryst.* 2015, C**71**, 3–8.

5. B. Ravel and M. Newville, *J*. *Synchrotron Radiat*. 2005, **12**, 537-541.

6. G. Kresse and J. Furthmuller, *Phys*. *Rev*. *B: Condens*. *Matter Mater*. *Phys*., 1996, **54**, 11169–11186.

7. G. Kresse and D. Joubert, *Phys*. *Rev*. *B: Condens*. *Matter Mater*. *Phys*., 1999, **59**, 1758–1775.

8. I. Hamada, *Phys*. *Rev*. *B: Condens*. *Matter Mater*. *Phys*., 2014, **89**, 121103.

9. Y. L. Wang, B. Li, S. Sarman, F. Mocci, Z. Y. Lu, J. Yuan, A. Laaksonen and M. D. Fayer, *Chem*. *Rev*., 2020, **120**, 5798–5877.